ICARUS 92, 252–262 (1991)

Ground-Based Infrared Measurements of the Global Distribution of Ozone in the Atmosphere of Mars

FRED ESPENAK,[1] MICHAEL J. MUMMA,[1] AND THEODOR KOSTIUK[1]

Planetary Systems Branch, Laboratory for Extraterrestrial Physics, NASA Goddard Space Flight Center, Greenbelt, Maryland 20771

AND

DAVID ZIPOY[1]

Astronomy Program, University of Maryland, College Park, Maryland 20742

Received October 22, 1990; revised March 18, 1991

We report measurements of the global distribution of ozone in the atmosphere of Mars, based on Doppler-limited infrared spectroscopy during the period 3–7 June 1988. The Martian spectrum was measured in the region of the P36 transition of $^{12}C^{16}O_2$ (1031.4774 cm^{-1}) in a search for two O_3 lines arising in the ν_3 band at 1031.4515 and 1031.4559 cm^{-1}. Surface pressures and temperature profiles were retrieved by inversion of the fully resolved $^{12}C^{16}O_2$ line. Ozone measurements were obtained at eight beam positions over a range of Martian latitudes (80° S to 20° N) and local solar hour angles (-0.5^h to $+5.5^h$). The total O_3 column abundance at each position was retrieved by fitting the lines with synthetic spectra generated by a radiative transfer program. The only previous ozone measurement at this season ($L_s \sim 204°$) was made above the south polar cap by Mariner 7 and revealed an abundance of 10 μm-atm. However, the retrieved O_3 column burdens of this investigation are less than 2.2 μm-atm for all latitudes sampled, consistent with seasonal abundances predicted by the models of Liu and Donahue, and Shimazaki and Shimizu.

INTRODUCTION

Ozone on Mars was first detected in absorption in the reflection spectrum of the south polar cap (L_s = 204°) using the Mariner 7 ultraviolet (UV) spectrometer (Barth and Hord 1971). A much more comprehensive study was performed with the Mariner 9 UV spectrometer from November 1971 through October 1972 (Barth *et al.* 1973). The observations were made during northern hemisphere winter–spring and southern hemisphere summer–fall (L_s = 292° to L_s = 102°) and showed that ozone exhibits large seasonal variations in the polar regions. In particular, the ozone abundance over the north polar cap attained a value of 16 μm-atm in late winter (i.e., 1 μm-atm = 10^{-6} m-am = 2.69×10^{15} molecules cm^{-2}) and decreased monotonically through spring. By the summer solstice, it had dropped below the spectrometer detection limit (3 μm-atm). Over the south polar cap, ozone first appeared in late summer and gradually increased to 6 μm-atm before the southern fall equinox. Ozone abundances as large as 57 μm-atm were measured in the north polar hood between 50° N and 75° N during late winter. Similarly, the maximum ozone abundance observed in the southern hemisphere (>30 μm-atm) was seen above the south polar hood between 50° S and 75° S during mid-fall. No ozone was observed within 40° latitude of the equator. Additional Mariner 9 observations of ozone showed a strong latitudinal variability which peaked at 60° N latitude during northern winter (Traub *et al.*, 1979). Ozone at any one location also exhibited large variations from day to day.

An analysis of the coappearance of ozone with clouds in the north polar hood (as seen in Mariner 9 television images) has demonstrated that a cold, clean, dry atmosphere is conducive to the presence of ozone (Barth and Dick 1974). The clouds are believed to be composed of water ice crystals which form when the temperature falls below ~180 K and, consequently, water vapor is condensed out of the atmosphere. Detailed observations of the seasonal and global distribution of water vapor using the Viking Orbiter MAWD instrument (Jakosky and Farmer 1982) show that water vapor varies from less than 1 to as much as 75 pr μm over an annual sublimation–condensation cycle. It vanishes from the atmosphere above the polar regions of the winter hemisphere and reappears

[1] Visiting astronomer at the Infrared Telescope Facility which is operated by the University of Hawaii under contract from the National Aeronautics and Space Administration.

0019-1035/91 $3.00

in early spring. The observed behaviors of O_3 and H_2O are supported by theoretical models of Martian photochemistry (McElroy and Donahue 1972, Parkinson and Hunten 1972) which predict that ozone is anticorrelated with the presence of odd hydrogen produced through water vapor photolysis:

$$h\nu + H_2O \rightarrow H + OH$$
$$H + O_3 \rightarrow OH + O_2.$$

However, in a theoretical study of Mars' global ozone distribution, Kong and McElroy (1977) find that H_2O alone is inadequate to explain completely the magnitude of meridional ozone variability. Their model indicates that another source of odd hydrogen is needed to produce H, OH, and HO_2, and they suggest H_2O_2. Like water, H_2O_2 also condenses out of the atmosphere at high latitudes in winter. Since gaseous H_2O and H_2O_2 abundances are subject to large temporal and spatial variations near their sublimation–condensation temperatures, the abundance of H varies likewise leading to the prediction that O_3 should exhibit similar variability. This is entirely consistent with Mariner 9 observations of significant ozone variability over localized regions and time scales of ≤ 1 day (Barth and Dick 1974, Traub *et al.* 1979).

Clearly, the temporal, spatial, and vertical distributions of O_3 and other key minor constituents (CO, O_2, H_2O, and H_2O_2) are all essential to discriminate among competing models and, ultimately, to improve our understanding of Mars' unique photochemistry, aeronomy, and evolution. Noxon *et al.* (1976) and Traub *et al.* (1979) have succeeded in making Earth-based measurements of Martian ozone indirectly through observations of O_2 dayglow emission which results from the ultraviolet photolysis of ozone. Although quite sensitive, these measurements had poor spatial resolution and their interpretation was strongly model dependent. The ultraviolet spectral signatures (Barth and Hord 1971, Barth *et al.* 1973) do not distinguish vapor phase O_3 from O_3 adsorbed on surfaces, and thus there have been no direct observations of O_3 in the gas phase on Mars. In this work, we report the first direct observations of gaseous ozone on Mars and measurements of its global distribution, acquired at high spatial resolution using the technique of infrared heterodyne spectroscopy.

OBSERVATIONS

Although the infrared spectrum of ozone has several strong rotational–vibrational bands, the measurement of Mars' ozone from ground-based observatories is severely hampered by terrestrial ozone (~3000 μm-atm) which renders Earth's atmosphere opaque at these frequencies. Fortunately, the geocentric radial velocity of Mars in the months before and after opposition Doppler shifts Martian ozone lines into the wings of their telluric counterparts where Earth's atmosphere is considerably more transparent. Given an instrument with resolving power sufficient to measure individual line profiles at sub-Doppler resolution, it then becomes possible to observe ozone lines directly in Mars' atmosphere. Infrared heterodyne spectrometers are well suited to this problem since they typically have a spectral resolving power of $\lambda/\Delta\lambda \sim 10^6$ at 10 μm. Heterodyne spectroscopy is accomplished by coherently mixing source radiation with the output of a laser local oscillator, and analyzing the difference frequency spectrum electronically. A more detailed description of the technique can be found in Mumma *et al.* (1982) and Kostiuk and Mumma (1983). Its applications to Mars are described in Mumma *et al.* (1981) and Deming *et al.* (1983, 1986).

The observations were made on June 3–7, four months prior to the 1988 opposition of Mars, using the Goddard Infrared Heterodyne Spectrometer (IRHS) at the coude focus of the 3-m NASA Infrared Telescope Facility (IRTF) atop Mauna Kea. Mars subtended an angle of 10.5 arc-sec, allowing good spatial mapping with a beam size of 0.8 arc-sec FWHM at 9.69 μm. At this time, Mars' southern hemisphere was experiencing mid-spring (L_s = 208°) when we would expect the ozone abundance to be dropping rapidly from its winter peak. Only one previous measurement has ever been made during this season (Mariner 7) and it revealed an ozone abundance of 10 μm-atm over the south polar cap. Our search concentrated on eight beam positions on the planet: 80° S, 60° S (three points), 40° S, 20° S, 0°, and 20° N. The 60° S measurements covered three different local solar hour angles (-0.5^h, $+2.5^h$, and $+5.5^h$) and provided diurnal information at high latitude where the greatest ozone abundance was anticipated. The basic observing geometry for Mars and the selected beam positions are shown in Fig. 1.

A typical observation sequence at one beam position on Mars consisted of 60 min of data, collected in 24 2.5-min integrations. Half of each integration cycle was spent viewing the disk of Mars and half spent viewing the adjacent sky 2 arc-min off the planet. Chopping between these two positions was accomplished at 13.5 Hz using the IRTF wobbling secondary. Switching between the Mars and sky beams was performed every two integrations to cancel possible baseline offsets due to differences in the two beams arising from the telescope and/or electronics. A 1273 K blackbody souce mounted on the IRHS optical table was measured several times each night, and was used to remove the instrumental response from the data. A dichroic beam splitter in the optical path fed a visible

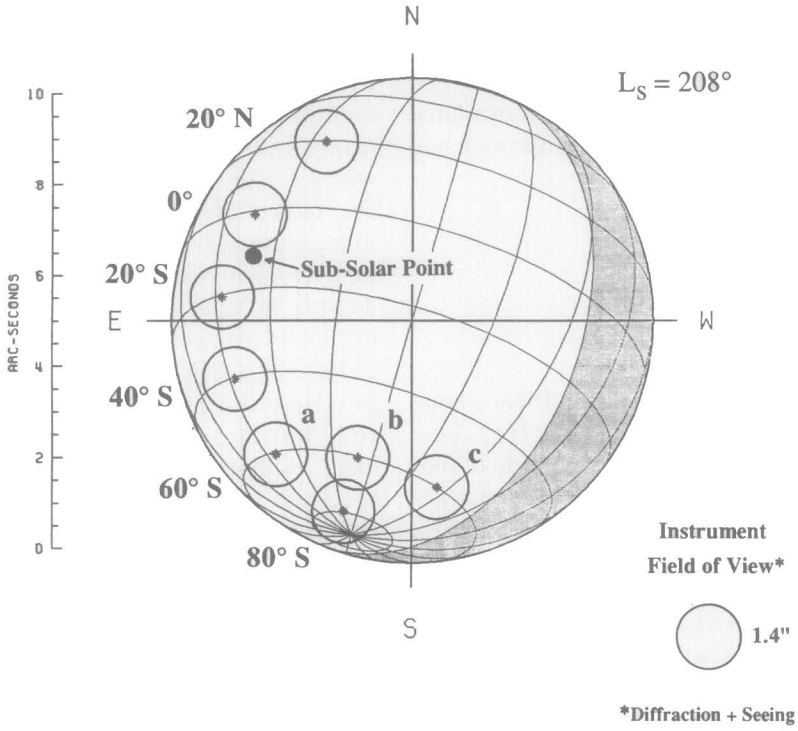

FIG. 1. Aspect geometry for Mars. In early June 1988, Mars subtended an angle of 10.5 arc-seconds and its southern hemisphere was experiencing mid-spring (L_s = 208°). Ozone measurements were made at eight beam positions on the planet: 80° S, 60° S (three points: a, b, and c), 40° S, 20° S, 0°, and 20° N. The observations at 60° S covered three different local solar hour angles (-0.5^h, $+2.5^h$, and $+5.5^h$, respectively) and provided diurnal information at high latitude where the greatest ozone abundance was anticipated.

image of the planet to a video camera. The image was simultaneously recorded and displayed on a television monitor overlaid by a time signal generator and an illuminated reticle which shows the system beam position and field of view. The videotaped image serves as a permanent record of telescope pointing accuracy and local seeing conditions during each observation. Pointing on Mars was accomplished using specially prepared transparent templates of the planet's observing geometry with desired beam positions (see Fig. 1) and scaled to the displayed video image. The templates were affixed to the video monitor and the telescope was actively guided by the observer during each integration. The refractive offset between the visual and the infrared images was also included. This procedure permitted the monitoring and adjustment of telescope guide rates which subsequently improved tracking and reduced the need for corrective guiding. An rms tracking uncertainty of ±0.5 arc-sec was achieved over one integration and visible seeing was typically ~1 arc-sec. Although infrared seeing is expected to be better than visible seeing, we had no way of directly measuring it. The field of view of the IRHS was matched to the nominal IRTF diffraction limit of 0.8 arc-sec (1.22 λ/D) at 9.69 μm. Adding these factors in quadrature, our effective instrumental beam width on the planet was about 1.4 arc-sec ($= \sqrt{[0.5^2 + 1.0^2 + 0.8^2]}$), corresponding to ~800 km on the planet.

DATA REDUCTION AND ANALYSIS

An FTS spectrum of Earth's atmospheric transmittance (Fig. 2, top) shows that the region from 1000 cm^{-1} to 1070 cm^{-1} is dominated by the ν_1 and ν_3 bands of ozone, making ground-based observations of extraterrestrial sources quite difficult. A high resolution synthetic transmittance spectrum of Earth at 1031.5 cm^{-1} (Fig. 2, bottom) shows a wealth of lines, all attributed to ozone. The strongest feature in this region is formed by a blend of two O_3 lines at 1031.4515 cm^{-1} and 1031.4559 cm^{-1} which both arise from the [000–001] band (positions shown as open circles). During early June 1988, the geocentric radial velocity of Mars was -11.8 km sec^{-1}. Thus, the same pair of ozone lines in Mars' spectrum were Doppler shifted 0.040 cm^{-1} higher in frequency where Earth's atmospheric transmittance is 50–60% (solid circles). For our observations, we tuned the $^{12}C^{16}O_2$ laser of the IRHS to the P36 line at 1031.477 cm^{-1} (9.69 μm). The spectrometer's spectral range is composed of 64 channels each 0.0008 cm^{-1} (25

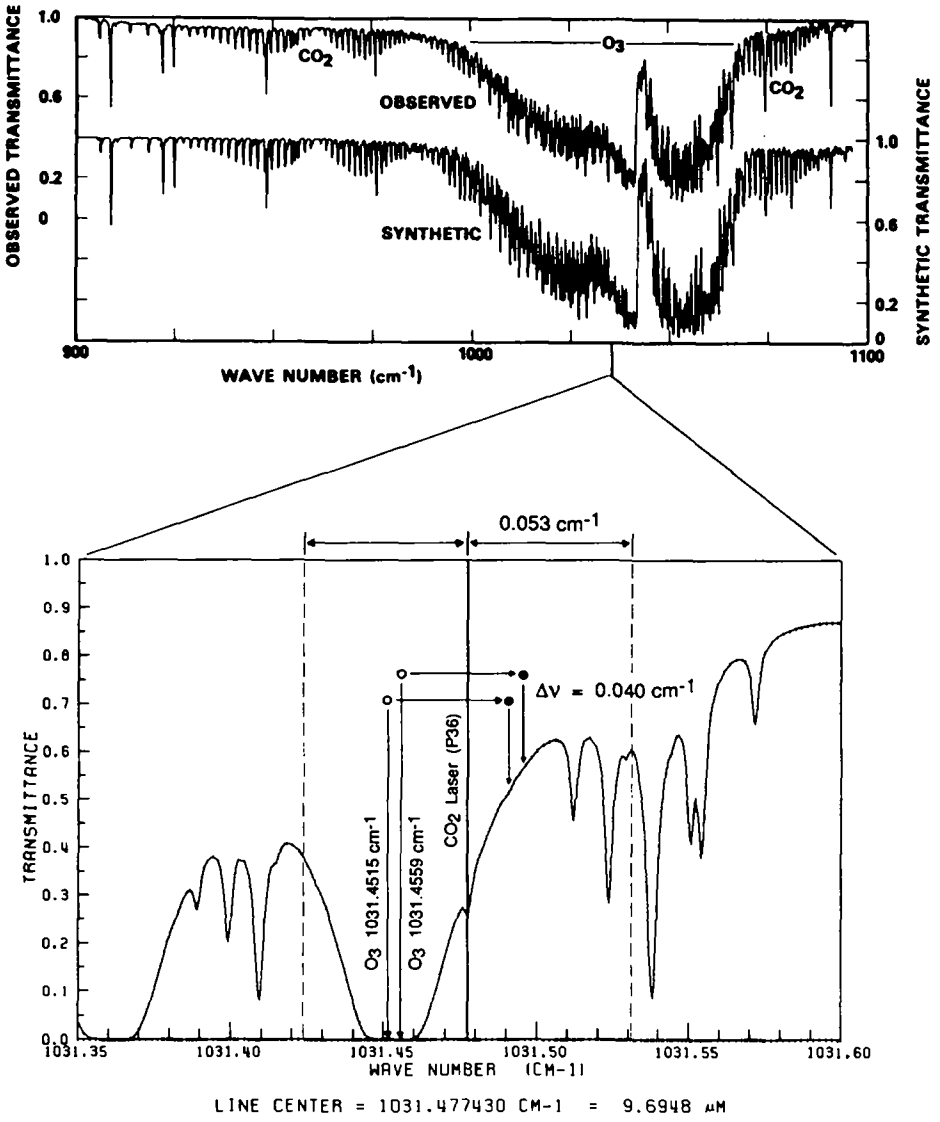

FIG. 2. The upper panel shows an observed FTS spectrum of Earth's atmospheric transmittance along with a synthetic spectrum (displaced for clarity). The spectral region from 1000 to 1070 cm^{-1} is dominated by the ν_1 and ν_3 bands of ozone, making extraterrestrial observations difficult. The lower panel shows a high resolution synthetic transmittance spectrum of Earth at 1031.5 cm^{-1} which is dominated by ozone. The strongest feature is formed by a blend of two ν_3 band O_3 lines at 1031.4515 cm^{-1} and 1031.4559 cm^{-1} (positions shown as open circles). During early June 1988, the geocentric radial velocity of Mars (− 11.8 km/sec) Doppler shifted these lines 0.040 cm^{-1} higher in frequency where Earth's atmospheric transmittance is 50–60% (solid circles). The GSFC heterodyne spectrometer was tuned to the CO_2 P36 line at 1031.4774 cm^{-1} (9.69 μm). The resultant spectrum is the sum of intensities from the upper and lower side bands (±0.053 cm^{-1}), symmetric about the CO_2 line.

MHz) wide and spaced contiguously over a 0.053 cm^{-1} (1600 MHz) interval. All channels were recorded simultaneously, thereby eliminating registration errors and drift. The resultant spectrum is the sum of intensities from the upper and lower side bands, symmetric about the CO_2 P36 laser position.

Each raw integration must be corrected for a number of effects before the Martian ozone abundance can be retrieved. First, the data must be divided by a blackbody spectrum in order to remove the IRHS instrumental response. Next, the effect of Earth's atmospheric transmittance must be removed, but this is more difficult because of its variability with frequency, time, and air mass. Each night, observations of the Moon (a thermal continuum source) were made at one or more different air masses to characterize the telluric transmittance. Although the Moon is hotter than Mars, its spectrum is not noise-free. Furthermore, it was not possible to observe the Moon at all desired air masses due to time constraints and low lunar declination during the run. Because of these factors,

a synthetic model of Earth's transmittance was developed using the lunar data. The lunar spectra were fitted with a plane parallel, 35 layer, radiative transfer model of Earth's atmosphere using molecular line parameters from the 1986 HITRAN database (Rothman *et al.* 1987). This database contains line positions and intensities of the ν_3 band of ozone measured by Flaud *et al.* (1987) from Fourier transform spectra. Uncertainties in the O_3 ν_3-band line positions are about 0.0003 cm^{-1} (Rinsland 1990). Due to uncertainties in the ozone sample purity, accuracies of line intensities are more difficult to determine but are estimated to be ±5%. The model atmosphere featured a temperature profile and surface pressure appropriate for local conditions atop Mauna Kea (altitude = 4200 m). By making small adjustments to the total column of ozone (~10%), good fits to the lunar data were achieved over the range of observed air masses.

The Mars integrations were then coadded in sets of four and the effects of the terrestrial atmosphere were removed through division by a synthetic transmittance spectrum at the corresponding air mass. Absolute flux calibration above the atmosphere was achieved by ratioing Mars spectra to Moon spectra, obtained on the same night and scaled for air mass via synthetic transmittances, and by adopting an appropriate temperature for the observed location on the lunar surface (Montgomery *et al.* 1966). The estimated uncertainty in the absolute flux calibration was ~5%. During the observing run, Mars' geocentric radial velocity decreased by +0.05 km s^{-1} (+0.002 cm^{-1}) per day and was modulated by the diurnal rotation of Earth which had an amplitude of ±0.43 km sec^{-1} (±0.0015 cm^{-1}) for the latitude of Mauna Kea and declination of Mars. Using an ephemeris based on the JPL DE 200 (Standish *et al.* 1982), each Mars integration set (= 10 min of data) was corrected for the topocentric Doppler shift. These sets could then be added together into groups of five to eight sets in order to improve the signal-to-noise ratio.

The final reduced spectra for the eight selected beam positions are displayed in Fig. 3 along with their relative positions on the planet. Additional information including the date, Universal Time, areocentric longitude, local solar hour angle, and integration time for each beam position is listed in Table I. The most obvious feature in each spectrum is the deep absorption line due to CO_2 P36 in the atmosphere of Mars. This line is optically thick ($\tau \sim$ 80 at line center) and is used to extract the atmospheric temperature profile by inversion of the radiative transfer equation at each beam position. In the absence of significant amounts of airborne dust (the primary source of continuum atmospheric opacity), the emergent intensity beyond the wings of the CO_2 line is a direct measure of thermal emission from the surface and is therefore a measure of the solid surface or ground temperature.

TABLE I
1988 Mars Ozone Observations

Beam position	Date/UT[a]	Areo-centric longitude	Solar hour angle	Integration time (min)	Surface temp. (K)	O_3 abundance (μm-atm)
80° S	3 June/17:29	158°	+1.7	35	212°	0.53
60° S a	4 June/14:51	143°	−0.5	60	248°	1.59
60° S b	6 June/16:24	99°	+2.5	70	236°	2.16
60° S c	6 June/14:23	28°	+5.5	80	227°	1.56
40° S	5 June/14:30	133°	- 0.8	50	244°	1.53
20° S	6 June/18:30	181°	−0.7	70	230°	1.42
00°	7 June/15:16	115°	−0.1	75	224°	1.55
20° N	5 June/17:33	155°	+0.7	85	229°	1.61

[a] Universal Time at midintegration.

Assuming an emissivity of 1, the retrieved surface temperatures range from 212 to 248 K and are consistent with temperatures obtained by the Mariner 9 and Viking orbiters (Kieffer *et al.* 1977). The predicted positions of the two ozone lines are indicated by the pair of downward pointing arrows above each spectrum (Fig. 3). Weak features at these positions are readily apparent in most of the spectra and are identified as Martian ozone.

Column abundances for ozone can be retrieved by fitting these lines with a synthetic spectrum. Naturally, the retrieved abundances are somewhat dependent on the model atmosphere used in the radiative transfer calculations. Fortunately, the adjacent CO_2 P36 line can be used to physically characterize the atmosphere at each beam position. This is accomplished as follows. The solid surface temperature measured directly from the spectra serves as the background continuum temperature at the base of the model atmosphere. An initial vertical temperature profile appropriate to the local time and latitude is then adopted (Hanel *et al.* 1972, Seiff and Kirk 1977, Seiff 1978, Conrath 1981). It includes a discontinuity of 20° to 30 K between the solid surface and gas surface temperature, in accordance with radiative equilibrium and spacecraft observations. A nominal surface pressure (7–9 mbar) is chosen based on the Martian season and areocentric latitude. The actual temperature profile is then retrieved through an analytic inversion of the observed lineshape using the radiative transfer equation, a multilayer atmospheric model, and a Voigt lineshape function. A plane parallel, 20-layer model atmosphere including the path geometry along the line of sight is used to model the CO_2, and the molecular line parameters are obtained from the 1986 HITRAN database. The CO_2 line core is typically formed at ~25 km. The distribution of contribution functions allows us to retrieve four to five values in the temperature profile in the bottom three scale heights of the atmosphere.

Temperature profiles were successfully retrieved for six of the eight spectra (Fig. 4). Unfortunately, the CO_2 lines

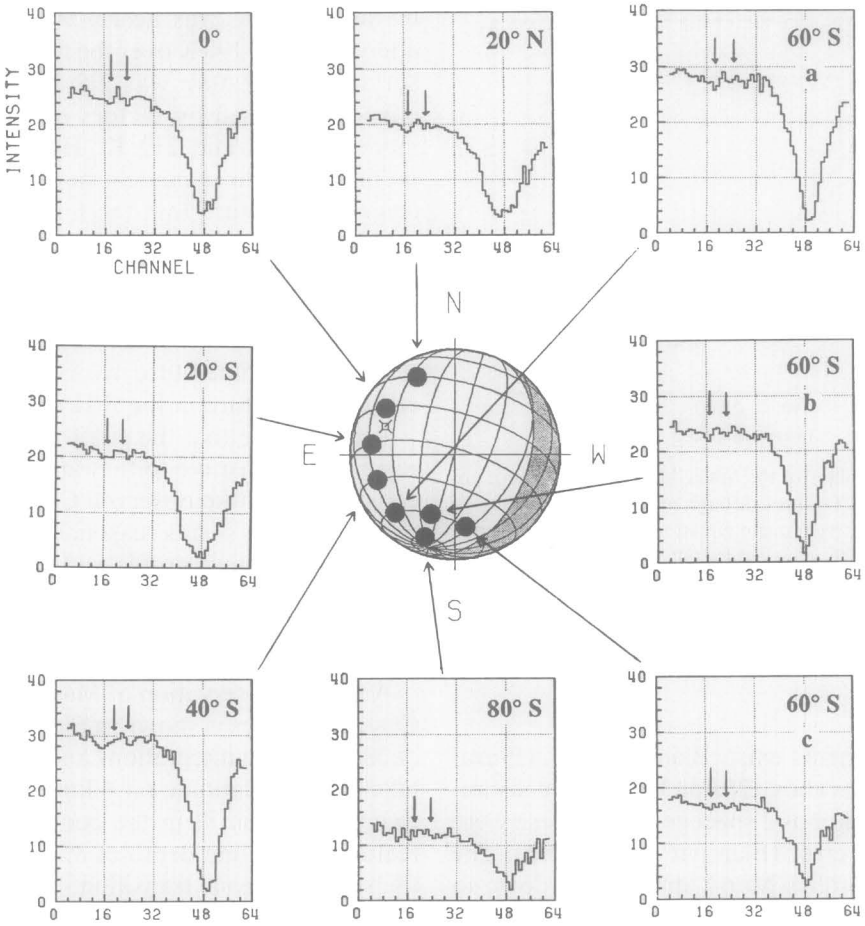

FIG. 3. Global distribution of O_3 in the atmosphere of Mars, 3–7 June 1988. The reduced 9.69-μm spectrum for each of the eight beam positions prominently exhibits the pressure-broadened $^{12}C^{16}O_2$ P36 absorption line in Mars' atmosphere. The positions of the O_3 lines in each spectrum are indicated with arrows. Absolute intensities are displayed in units of ergs/(cm^{+2}*sec*sr*cm^{-1}) while the abscissa indicates the spectrometer channel number. Each channel is 0.00083 cm^{-1} wide and the origin is at 1031.4774 cm^{-1}. The basic aspect geometry of Mars in June 1988 and the relative beam positions of each spectrum are shown at the center of the figure.

observed at the two remaining beam positions (20° N and 20° S) were contaminated by terrestrial ozone lines which could not be completely removed. In these two cases, the retrieved temperature profile from the adjacent equatorial beam position was adopted. Uncertainties in the retrieved temperature profiles were evaluated by adding random Gaussian noise (scaled to that observed in the continuum) to the synthetic spectra which were then inverted to retrieve a new temperature profile. This process was repeated 25 times in order to create a large enough sample to generate RMS statistics on the retrieved temperature profiles. The typical 1 σ error bars on the temperature profile retrieved for 60° S data are $\pm$3.5 K at the surface, and monotonically decrease to $\pm$1.5 K at an altitude of 30 km (Fig. 4). Four of the six retrieved temperature profiles resemble the Viking descent measurements (Seiff and Kirk 1977), although they are 5 to 10 K colder. The 80° S profile has a nearly isothermal temperature of 192 to 186 K in the first two scale heights, consistent with Mariner 9 IRIS data for high latitudes (Hanel *et al.* 1972, Conrath 1981). The 40° S profile exhibits a rapid drop in temperature in the first scale height before becoming isothermal at ~167 K. Such cold temperature profiles at midlatitudes have been observed before (Clancy *et al.* 1990) and are consistent with radiative calculations of a dust-free atmosphere. It should be pointed out that the retrieved temperature profiles each represent a mean profile integrated over approximately 1 hr and covering ~15° of latitude, >30° of longitude, and a range of surface topography.

After the physical parameters of the atmosphere are determined from the measured CO_2 lineshape, the ozone lines are fitted by varying the total column abundance along the line of sight. The vertical mixing ratio of O_3 is unknown at present. Theoretical altitude profiles for ozone have been published (McElroy and Donahue 1972, Parkinson and Hunten 1972, Kong and McElroy 1977),

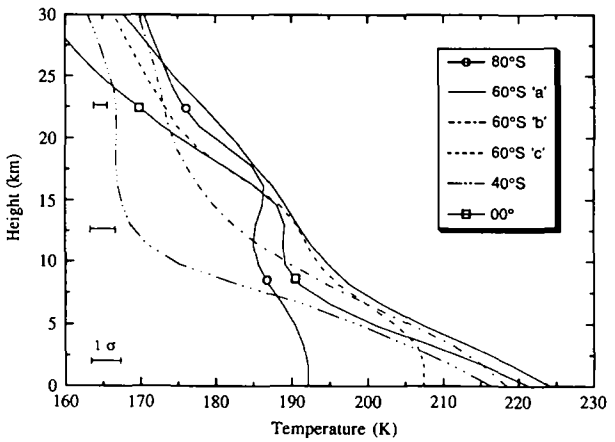

FIG. 4. Temperature profiles of the lower Martian atmosphere are derived from the observed CO_2 lines through an analytic inversion of the lineshapes using the radiative transfer equation. The typical 1 σ error bars on the temperature profile retrieved for 60° S data are ±3.5 K near the surface and monotonically decreasing to ±1.5 K at an altitude of 30 km. The retrieved solid surface temperatures are given in Table I and are warmer than the atmospheric temperature near the surface.

but no direct measurements exist. Blamont *et al.* (1989a) reported vertical profiles above 25 km, based on measurements made from the Phobos 2 spacecraft, but these were later reported to be in error (Blamont *et al.* 1989b). The current investigation probes Mars' atmosphere down to the surface, but our retrievals are insensitive to the vertical distribution for ozone because of insufficient signal-to-noise which prevents us from measuring the lineshape of the observed O_3 lines. Thus, we have adopted a uniform vertical mixing ratio for O_3 in our model atmosphere. Uncertainties in the retrieved ozone abundances were determined by adding random Gaussian noise (scaled to that observed in the continuum) to the modeled synthetic spectrum which was then fit iteratively to generate RMS statistics. Uncertainties in the retrieved temperature profiles were found to be of little consequence (<5%) to the derived ozone abundances.

The observed 9.69-μm spectrum is actually composed of two components: (1) the transmitted intensity of the thermal background (i.e., solid surface of Mars) which undergoes selective absorption and scattering as it passes through the Martian atmosphere, and (2) the self-emission due to the atmosphere. In cases where the temperature of the solid surface is equal to or less than the overlying gas (i.e., an inversion), the self-emission of the gas can "fill in" the absorption line, resulting in a shallower and more difficult feature to measure. Since the temperature profile above the polar regions of Mars can be isothermal or exhibit inversions in the first scale height, we investigated the effects of several models on the 80° S latitude spectrum. The temperature profile retrieved through inversion of the CO_2 line was nearly isothermal with a value of approximately 190 K over the first 15 km and the observed surface temperature was 212 K. Retrieved ozone abundances increased by factors of 2 and 30 for isothermal models of 202 and 212 K. However, the self-emission predicted by these models so severely modified the CO_2 absorption feature that the hotter isotherms were ruled out from further consideration. Similarly, the CO_2 line could not be fit when introducing a temperature inversion in the first scale height. Although the vertical resolution is no better than one-half scale height, the CO_2 line is sensitive to temperature inversions which change the average temperature in the first scale height.

We conclude that the retrieved ozone abundances are relatively insensitive to the range of temperature profiles constrained by the observed CO_2 absorption line. An upper limit of 5% seems reasonable for the uncertainty due to the temperature profile variations.

RESULTS AND DISCUSSION

A typical observation of Mars with retrieved fits to the CO_2 and O_3 lines is shown in Fig. 5. The spectrum consists of 28 individual integrations and represents 70 min of data taken at 60° S latitude on 4 June at 14:51 UT. The signal-to-noise ratio is 33 in the continuum and an absorption feature with a line depth of 8% is seen at the position of the stronger ozone transition. The retrieved ozone abundance at this position is 1.59 μm-atm with an rms error of ±0.37 μm-atm. For comparison, synthetic ozone lines have also been modeled with total column abundances of 5, 10, and 20 μm-atm. An ozone abundance of 10 μm-atm is equal to that seen by Mariner 7 above the south polar cap during the same season and results in a modeled line depth of 40%.

A summary of the retrieved ozone abundances for all eight beam positions is given in Fig. 6 and is listed in Table I. The typical rms error of the retrieved O_3 abundance is ±0.4 μm-atm. In no case does the abundance exceed 2.2 μm-atm. Based on Mariner 7 observations, we expected to find the greatest ozone abundance (on the order of 10 μm-atm) at high southern latitudes. The photochemical model of Kong and McElroy (1977) cannot be compared directly with our observations because the model was calculated only for the seasons L_s = 348° and L_s = 38°, while our data were obtained at L_s = 208°. Nevertheless, if one assumes symmetry in the seasonal variation of ozone in the northern and southern hemispheres, this model suggests that highest ozone abundances occur at high latitudes in the winter hemisphere which rapidly diminish with the onset of spring, just as observed by Mariner 9. Surprisingly, the 80° S latitude position in our investigation actually yielded the lowest O_3 abundance with an upper limit of 0.5 μm-atm. The three points at 60° S lati-

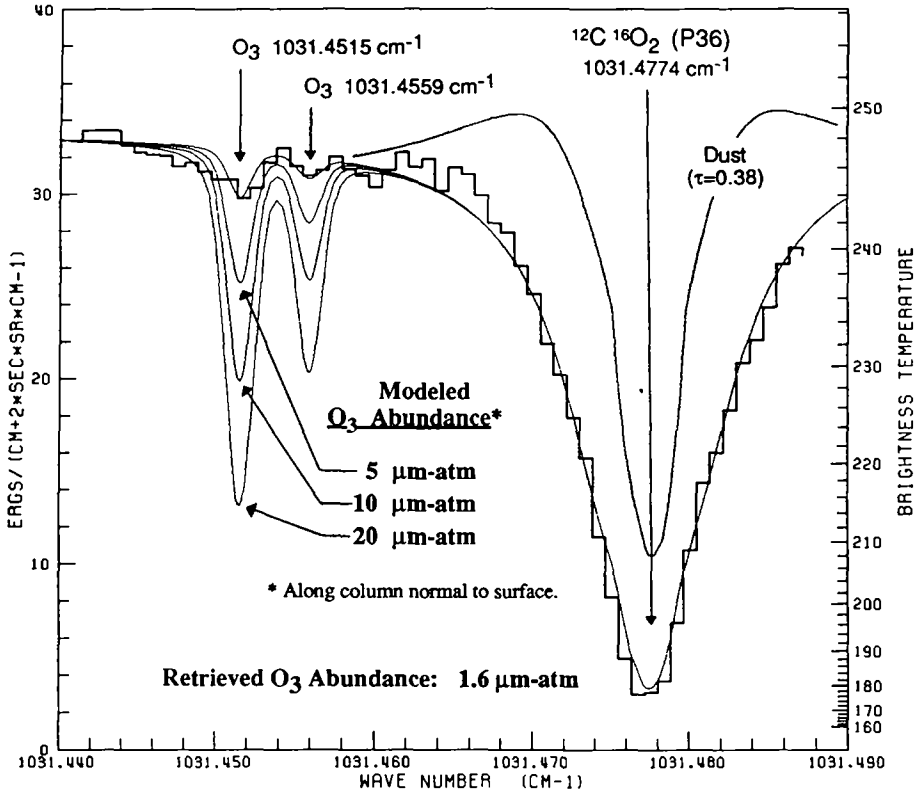

FIG. 5. Ozone line strength vs abundance, 4 June 1988, 14:51 UT. A typical spectrum consisting of 70 min of data taken at 60° S latitude (position a) is shown with retrieved fits to the CO_2 and O_3 lines. The absorption feature at the position of the stronger ozone transition yields a retrieved ozone abundance of 1.59 μm-atm with an rms error of ± 0.37 μm-atm. For comparison, synthetic ozone lines have also been modeled with total column abundances of 5, 10, and 20 μm-atm. Also shown is a synthetic spectrum using a dusty atmosphere model whose continuum optical depth (τ = 0.38) was adjusted until the observed ozone lines were fit with an assumed abundance of 10 μm-atm. Though forced to fit the ozone line, the fit to CO_2 is grossly inadequate, demonstrating that a dusty atmosphere model is not appropriate.

tude showed the maximum abundance ranging between 1.56 and 2.16 μm-atm. No significant variation was seen at this latitude in spite of the fact that the data were taken on two separate days and covered local solar hour angles of -0.5^h, $+2.5^h$, and $+5.5^h$. The remaining four points all lie within 1 hr of local apparent noon and have O_3 abundances between 1.4 and 1.6 μm-atm. These results retrieve far less ozone at the high southerly latitudes than initially anticipated. We now examine several possible explanations for these observations.

During the 1988 apparition of Mars, the International Mars Patrol (a worldwide network of amateur astronomers) monitored the planet, recording the location and appearance of phenomena in the Martian atmosphere. As early as April 1988, minor dust storms and clouds were observed, sketched, and/or photographed. On June 3, a large dust storm appeared in the Hellas basin (ϕ = 50° S, λ = 290°) which eventually extended at least 90° in longitude and persisted until June 21 (Eicher 1988). During the same month, Japanese observers reported a number of localized dust storms scattered around the planet. Some observers reported a yellowish haze covering the south polar cap until mid-July. Although none of these events directly triggered a major global dust storm, they suggest that the atmosphere of Mars may have contained substantial amounts of dust during this investigation. In a detailed series of calculations on the effects of airborne dust on ozone, Lindner (1988) found that typical dust abundances induce 10–50% increases in O_3 abundances due to the dust's masking of photodissociative ultraviolet photons. However, he pointed out that reflectance spectroscopy techniques at ultraviolet wavelengths may have difficulty observing these increases since the large optical depths of aerosols effectively hide the greatest ozone concentrations from such measurements.

While our 40° S temperature profile and the observations of Clancy *et al.* (1990) both point toward a dust-free atmosphere during the 1988 opposition, visual and photographic observations unequivocally demonstrate the presence of some dust. To investigate whether airborne dust could be masking ozone in the high southern latitude data, a "gray" dust was added to the radiative transfer model. Although silicate dust exhibits a structured absorption feature near 9 μm, the gray dust assump-

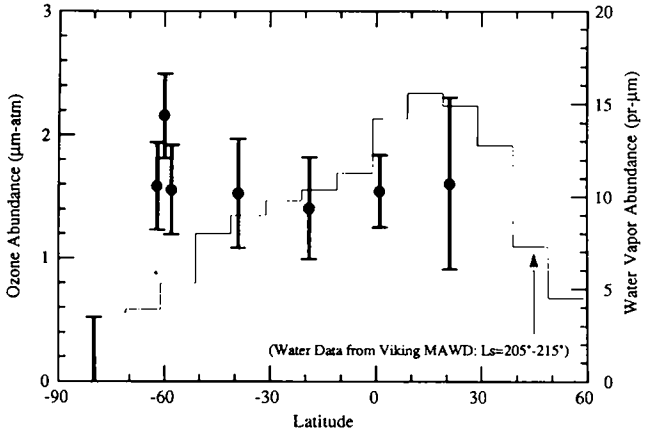

FIG. 6. Retrieved ozone abundances for all eight beam positions reveals a peak abundance of 2.16 μm-atm. The 80° S latitude position included the south polar cap (SPC) but actually yielded the lowest O_3 burden with an upper limit of 0.54 μm-atm. This is puzzling since Mariner 7 measured an O_3 abundance of 10 μm-atm above the SPC. The three points at 60° S latitude actually showed the maximum abundance ranging between 1.56 and 2.16 μm-atm. No significant variation was seen at this latitude in spite of the fact that the data were taken on two separate days and covered a range of local solar hour angles. A histogram of Viking Orbiter MAWD measurements of the latitudinal distribution of water vapor averaged over 10° latitude strips for L_s = 205–215° (after Jakosky and Farmer 1982) shows that the water vapor abundance reached a maximum of 15.5 pr μm near the equator and decreased to a minimum of 3.7 pr μm at high southern latitudes.

tion is valid since our band pass is so narrow (~0.1 cm^{-1}). Using a range of optical depths ($0.2 < \tau < 2.0$) characterizing observed Martian dust (Toon *et al.* 1977), fits were attempted assuming an O_3 abundance of 10 μm-atm. When the optical depth of the dust is between 0.4 and 0.9, reasonably good fits to the ozone are obtained because the lower atmosphere is effectively masked. However, that same region of the atmosphere is largely responsible for the formation of the wings of the CO_2 absorption lines and the synthetic spectra are no longer consistent with observed CO_2 lineshapes (Fig. 5). Thus, we reject dust opacity as a mechanism for lowering the observed O_3 abundances.

Using data from the Auguste-Spectrophotometer Interferometer experiment aboard the Phobos 2 spacecraft, Atreya and Blamont (1990) suggest that heterogeneous chemistry on airborne dust and water ice grains may play a significant and previously underestimated role in reformation of CO_2 and may contribute to other photochemical processes. However, laboratory measurements of sticking coefficients and rate constants are needed in order to evaluate the importance of dust as sites for heterogeneous chemistry in the Martian atmosphere. While no direct evidence exists linking heterogeneous chemistry with ozone variability, it cannot be entirely ruled out.

However, since ozone and water are known to be strongly anticorrelated with each other, a more obvious explanation lies in the water vapor content of the Martian atmosphere during the ozone observations. A histogram of Viking Orbiter MAWD measurements of the latitudinal distribution of water vapor averaged over 10° latitude strips for L_s = 205–215° exhibits a minimum (3.7 pr μm) in water vapor at high southern latitudes and a maximum (15.5 pr μm) near the equator (Fig. 6). Water vapor measurements of Mars' atmosphere made concurrently with this investigation (Rizk *et al.* 1990) are in qualitative agreement with MAWD data for the same season. Detailed comparison and modeling with the Rizk *et al.* H_2O observations will be presented in a future paper. With the characteristic latitudinal water vapor distribution established, we can compare our ozone observations with several theoretical models in the published literature.

Ozone abundances have been calculated by Liu and Donahue (1976) for five H_2O concentrations, using a steady state model which simulates conditions over the polar cap during spring. Ignoring surface losses, they predict O_3 abundances of 2.0 and 0.92 μm-atm for H_2O concentrations of 3.7 and 15 pr μm, respectively. If the surface acts as a perfect sink, removing all ozone upon direct contact, then an O_3 abundance of 2.0 μm-atm is reduced to 0.7 μm-atm. Thus the modelled ozone abundances in good agreement with measured values, given the range of H_2O concentrations and uncertainties in surface losses.

Shimazaki and Shimizu (1979) have developed a one-dimensional, time-dependent model of the seasonal variability of ozone on Mars at a latitude of 65°. Input data for the model include seasonal variations in the atmospheric temperature, pressure, and water vapor abundance obtained by Viking. Some previous models (McElroy and Donahue 1972, Parkinson and Hunten 1972) have adopted relatively arbitrary mixing ratios of HO_x which directly affect predicted ozone abundances. In contrast, the Shimazaki–Shimizu (SS) model computes odd hydrogen (H, OH, HO_2) concentrations simultaneously from their chemical rate equations assuming photochemical equilibrium and Viking H_2O abundances. Since solutions for the O_x and HO_x systems are obtained through iteration, the odd oxygen and odd hydrogen compounds are fully interactive in the model. Surface losses are considered as well as two different vertical transport rates.

In general, higher O_3 abundances are expected at times when the odd oxygen production rate is high and the water vapor column abundance is low. For the northern hemisphere, the SS model finds that these conditions are met at two seasons: L_s = 220° and L_s = 330°. However, L_s = 220° is not expected to exhibit much ozone because the model also predicts a large HO_2 density at that season (early winter). To summarize, the SS model predicts that maximum ozone density occurs not at winter solstice but

rather during late winter, when the amount of H_2O is still small. This behavior is due to a combination of the seasonal variations in water vapor content and odd oxygen production rate in the lower atmosphere. Water vapor levels correlate with temperatures which reach a minimum at $L_s = 290°$ (northern hemisphere), whereas odd oxygen production rates are essentially symmetric about the winter solstices ($L_s = 270°$ in northern hemisphere). Although Mariner 9 ozone measurements cover only half of one Martian year, comparison with SS model predictions are quite favorable for both northern and southern hemispheres. One significant departure of the model is the failure to predict the sharp rise in ozone abundance seen in the northern hemisphere in early summer ($L_s = 50°$). The SS model predicts that minimum ozone abundance (≤ 2 μm-atm) at 65° N latitude should occur from $L_s = 50°$ to $L_s = 210°$ and at 65° S latitude from $L_s = 210°$ to $L_s = 30°$. This is entirely consistent with the present results of an ozone abundance between 1.5 and 2.2 μm-atm at 60° S latitude ($L_s = 208°$).

The puzzle remains as to why Mariner 7 saw some 20 times more ozone above the South Polar Cap (SPC) than was measured by this investigation. We suspect it to be a consequence of the vastly different fields of view of the two respective instruments and the fact that ozone exhibits large spatial variability (Barth and Dick 1974, Traub *et al.* 1979). During its closest approach to Mars, the Mariner 7 UV spectrometer viewed a narrow strip 10 by 100 kilometers so that only a small section of the SPC filled its field of view. In contrast, the southern-most IRHS beam (centered on 80° S) took in an area including 70° S to 90° S latitude and effectively covered a region hundreds of times larger. The receding SPC underfilled our beam by a factor of ~4. If we assume that the large ozone abundance seen by Mariner 7 is localized, then two factors would work toward minimizing our retrieved ozone abundance. The first effect would be due to beam dilution resulting directly from the ratio of the physical areas observed by the two instruments. Second, since the SPC is colder and radiates less thermal infrared energy than the surrounding regions, this serves to further dilute the beam by lowering the thermal contrast between the SPC and the surrounding warmer regions. These arguments are supported by an observed surface temperature of 212 K at the 80° S point (Table I), whereas the SPC should have a temperature at least as cold as the condensation point of CO_2 (i.e., 148 K at 7 mbar). One final point to consider is that the UV reflectance spectroscopy technique used by both Mariners 7 and 9 is incapable of distinguishing between gaseous ozone and ozone adsorbed by CO_2 ice (Barth and Hord 1971). In contrast, our investigation is only sensitive to atmospheric ozone. Thus, the large discrepancies we see between our data and the Mariner 7 observations may suggest that a significant fraction of the ozone seen by Mariner 7 was adsorbed onto Mars' SPC or onto airborne ice crystals.

CONCLUSION

Infrared O_3 lines at 9.69 μm in Mars' atmosphere was measured for eight beam positions over a range of Martian latitudes (80° S to 20° N) and local solar hour angles (-0.5^h to $+5.5^h$). The total O_3 column abundance at each position was retrieved through line fits with synthetic spectra generated by a radiative transfer program using a 20 layer plane parallel model atmosphere. The retrieved O_3 column burdens were found to be less than 2.2 μm-atm at all positions sampled. The results are consistent with midspring ($L_s \sim 204°$) abundances predicted by the photochemical models of Liu and Donahue, and Shimazaki and Shimizu. Both models attribute ozone variability to seasonal variations in the atmospheric concentration of odd hydrogen (H, OH, HO_2 created from photolysis of H_2O, H_2O_2) which destroys ozone ($H + O_3 \rightarrow OH + O_2$). However, additional measurements at high spatial resolution are needed at other seasons to confirm the details of temporal and global variability predicted by these models. Assessment of the role of heterogeneous chemistry in controlling ozone variability awaits laboratory measurements of the appropriate rates and additional synthetic modeling.

Infrared heterodyne spectroscopy has proven to be a useful technique in making direct ground-based observations of Martian ozone. We plan to continue this work by measuring the global distribution of ozone during other seasons at future oppositions of Mars.

ACKNOWLEDGMENTS

The authors thank the staff of NASA Infrared Telescope Facility for their invaluable technical and logistical support. We would also like to extend our gratitude and appreciation to the many amateur observers of the International Mars Patrol, and especially to Mars Recorders Jeff C. Beish and Donald C. Parker (Association of Lunar and Planetary Observers) for coordinating this network. This work was supported by the NASA Solar System Exploration Division, Planetary Astronomy Program under RTOP 196-41-54.

REFERENCES

ATREYA, S. K., AND J. E. BLAMONT 1990. Stability of the Martian atmosphere: Possible role of heterogeneous chemistry. *Geophys. Res. Lett.* **17,** 287–290.

BARTH, C. A. 1985. In *The Photochemistry of Atmospheres. Earth, the Other Planets, and Comets* (J. Levine, Ed.), Academic Press, New York.

BARTH, C. A., AND M. L. DICK 1974. Ozone and the polar hood of Mars. *Icarus* **22,** 205–211.

BARTH, C. A. AND C. A. HORD 1971. Mariner ultraviolet spectrometer: Topography and polar cap. *Science* **173,** 197–201.

BARTH, C. A., C. A. HORD, A. I. STEWART, A. L. LANE, M. L. DICK, AND G. P. ANDERSON 1973. Mariner 9 ultraviolet spectrometer experiment: Seasonal variation of ozone on Mars. *Science* **179,** 795–796.

BLAMONT, J. E., E. CHASSEFIERE, J. P. GOUTAIL, B. MEGE, M. NUNES-PINHARANDA, G. SOUCHON, V. A. KRASNOPOLSKY, A. A. KRYSKO, AND V. I. MOROZ 1989a. Vertical profiles of dust and ozone in the Martian atmosphere deduced from solar occultation measurements. *Nature* **341,** 600–602.

BLAMONT, J. E., E. CHASSEFIERE, J. P. GOUTAIL, B. MEGE, M. NUNES-PINHARANDA, G. SOUCHON, V. A. KRASNOPOLSKY, A. A. KRYSKO, AND V. I. MOROZ 1989b. In *First Results of the Phobos–Mars Mission and Future Space Exploration of Mars, Paris, 23–27 October.*

CLANCY, R. T., D. O. MUHLEMAN, AND G. L. BERGE 1990. Global changes in the 0–70 km thermal structure of the Mars Atmosphere derived from 1975 to 1989 microwave CO spectra. *J. Geophys. Res.* **95,** 14,543–14,554.

CONRATH, B. J. 1981. Planetary-scale wave structure in the Martian atmosphere. *Icarus* **48,** 246–255.

DEMING, D., F. ESPENAK, D. JENNINGS, T. KOSTIUK, M. MUMMA, AND D. ZIPOY 1983. Observations of the 10-μm natural laser emission from the mesospheres of Mars and Venus. *Icarus* **55,** 347–355.

DEMING, D., M. J. MUMMA, F. ESPENAK, AND T. KOSTIUK 1986. Polar warming in the middle atmosphere of Mars. *Icarus* **66,** 366–379.

EICHER, D. J. 1989. Mars' opening act. *Astronomy*, December 1988, 76–79.

FLAUD, J.-M., C. CAMY-PEYRET, V. MALATHY DEVI, C. P. RINSLAND, AND M. A. H. SMITH 1987. The ν_1 and ν_3 bands of $^{16}O_3$: Line positions and intensities. *J. Mol. Spectrosc.* **124,** 209–217.

HANEL, R., B. CONRATH, W. HOVIS, V. KUNDE, P. LOWMAN, W. MAGUIRE, J. PEARL, J. PIRRAGLIA, C. PRABHAKARA, B. SCHLACHMAN, G. LEVIN, P. STRATT, AND T. BURKE 1972. Investigation of the Martian environment by infrared spectroscopy on Mariner 9. *Icarus* **17,** 423–442.

HESS, S. L., J. A. RYAN, J. E. TILLMAN, R. M. HENRY, AND C. B. LEOVY 1980. The annual cycle of pressure on Mars measured by Viking Landers 1 and 2. *Geophys. Res. Lett.* **7,** 197–200.

HUNTEN, D. M. 1974. Aeronomy of the lower atmosphere of Mars. *Rev. Geophys. Space Res.* **12,** 529–535.

JAKOSKY, B. M., AND C. B. FARMER 1982. The seasonal and global behavior of water vapor in the Mars atmosphere: Complete global results of the Viking atmospheric water detector experiment. *J. Geophys. Res.* **87,** 2999–3019.

KIEFFER, H. H., T. Z. MARTIN, A. R. PETERFREUND, B. M. JAKOSKY, E. D. MINER, AND F. D. PALLUCONI 1977. Thermal and albedo Mapping of Mars during the Viking primary mission. *J. Geophys. Res.* **82,** 4249–4291.

KONG, T. Y. AND M. B. MCELROY 1977. The global distribution of O_3 on Mars. *Planet. Space Sci.* **25,** 839–857.

KOSTIUK, T., AND M. J. MUMMA 1983. Remote sensing by infrared heterodyne spectroscopy. *Appl. Opt* **22,** 2644–2654.

LANE, A. L., C. A. BARTH, C. A. HORD, AND A. I. STEWART 1973. Mariner 9 ultraviolet spectrometer experiment: Observations of ozone on Mars. *Icarus* **18,** 102–108.

LINDNER, B. L. 1988. Ozone on Mars: The effects of clouds and airborne dust. *Planet. Space Sci.* **36,** 125–144.

LIU, S. C. AND T. M. DONAHUE 1976. The regulation of hydrogen and oxygen escape from Mars. *Icarus* **28,** 231–246.

MCELROY, M. B., AND T. M. DONAHUE 1972. Stability of the Martian atmosphere. *Science* **177,** 986–988.

MCELROY, M. B., T. Y. KONG, AND Y. L. YUNG 1977. Photochemistry and evolution of Mars' atmosphere: A Viking perspective. *J. Geophys. Res.* **82,** 4379–4388.

MCELROY, M. B., AND J. C. MCCONNELL 1971. Dissociation of CO_2 in the Martian atmosphere. *J. Atmos. Sci.* **28,** 879–884.

MONTGOMERY, C. G., J. M. SAARI, R. W. SHORTHILL, AND N. F. SIX, JR. 1966. *Directional Characteristics of Lunar Thermal Emission* Technical Note R-13, Boeing Document B1-8L-0568. Brown Engineering Co., Inc. Huntsville, AL.

MUMMA, M. J., D. BUHL, G. CHIN, D. DEMING, F. ESPENAK, T. KOSTIUK, AND D. ZIPOY 1981. Discovery of natural gain amplification in the 10 μm CO_2 laser bands on Mars: A natural laser. *Science* **212,** 45–49.

MUMMA, M. J., T. KOSTIUK, D. BUHL, G. CHIN, AND D. ZIPOY 1982. Infrared heterodyne spectroscopy. *Opt. Eng.* **21,** 313–319.

NOXON, J. F., W. A. TRAUB, N. P. CARLETON AND P. CONNES 1976. Detection of O_2 dayglow emission from Mars and the Martian ozone abundance. *Astrophys. J.* **207,** 1025–1035.

PARKINSON, T. D., AND D. M. HUNTEN 1972. Spectroscopy and aeronomy of O_2 on Mars. *J. Atmos. Sci.* **29,** 1380–1390.

RINSLAND, C. P. 1990. Private communication.

RIZK, B., W. K. WELLS, D. M. HUNTEN, C. R. STOKER, R. S. FREEDMAN, T. ROUSH, J. B. POLLACK, AND R. M. HABERLE 1990. Meridional Martian water abundance profiles during the 1988–89 season. *Icarus*, in press.

ROTHMAN, L. S., R. R. GAMACHE, A. GOLDMAN, L. R. BROWN, R. A. TOTH, H. M. PICKETT, R. L. POYNTER, J. M. FLAUD, C. CAMY-PEYRET, A. BARBE, N. HUSSON, C. P. RINSLAND, AND M. A. H. SMITH 1987. The HITRAN database: 1986 edition. *Appl. Opt* **26,** 4058–4097.

SEIFF, A. 1978. In *The Mars Reference Atmosphere* (A. J. Kliore, Ed.). Pergamon Press, Oxford.

SEIFF, A., AND D. B. KIRK 1977. Structure of the atmosphere of Mars in summer at mid-latitudes. *J. Geophys. Res.* **82,** 4364–4378.

SHIMAZAKI, T. 1981. A model of temporal variations in ozone density in the Martian atmosphere. *Planet. Space Sci.* **29,** 21–33.

SHIMAZAKI, T., AND M. SHIMIZU 1979. The seasonal variation of ozone density in the Martian atmosphere. *J. Geophys. Res.* **84,** 1269–1276.

STANDISH, JR., E. M. 1982. Orientation of the JPL ephemerides, DE 200/LE 200, to the dynamical equinox of J 2000. *Astron. Astrophys.* **114,** 297–302.

TOON, O. B., J. B. POLLACK, AND C. SAGAN 1977. Physical properties of the particles composing the Martian dust storm of 1971–1972. *Icarus* **30,** 663–696.

TRAUB, W. A., N. P. CARLETON, P. CONNES, AND J. F. NOXON 1979. The latitude variation of O_2 dayglow and O_3 abundance on Mars. *Astrophys. J.* **229,** 846–850.

WEHRBEIN, W. M., C. W. HORD, AND C. A. BARTH 1979. Mariner 9 ultraviolet spectrometer experiment: Vertical distribution of ozone on Mars. *Icarus* **38,** 288–299.